International Journal of Environmental Sciences
ISSN: 2229-7359
Vol. 11 No. 20s, 2025
https://theaspd.com/index.php

Tailored PANI/Tio$_2$ Nanocomposites: Influence Of Tio$_2$ Loading On The Photocatalytic And Antimicrobial Behaviour

P. Jenifer[1], P. Rajesh Anantha Selvan[2], M. PraveenDaniel[3]
[1]Research Scholar (20121272032006), Department of Chemistry, St. John's College, Palayamkottai, Tirunelveli, Affiiated to Manonmaniam Sundaranar University, Tirunelveli, Tamil Nadu, India.
[2]Associate Professor, Department of Chemistry, St. John's College, Palayamkottai, Tirunelveli, Affiliated to Manonmaniam Sundaranar University, Tirunelveli, Tamil Nadu, India.
[3]Department of Chemistry, Francis Xavier Engineering College, Palayamkottai, Tirunelveli, Tamil Nadu, India – 627003
Corresponding Author Email: rajesh.chem@st.johnscollege.edu.in

Abstract
PANI/TiO_2 nanocomposite composites with different TiO_2 weight percentages were synthesized by in-situ chemical oxidative polymerization method. Polymerization of aniline using ammonium persulfate (APS) in acidic medium at room temperature for the PANI/TiO_2 nanocomposite. The nanocomposites were characterized by using PXRD, FTIR, UV-Vis, SEM and EDS. SEM images reveal that the samples exhibit a spherical morphology, with particle sizes for the various TiO_2-loaded samples measured at 26 nm, 19 nm, 25 nm, and 24 nm, respectively. FTIR analysis shows the functional groups related to PANI and TiO_2. Further the photocatalytic activity of nanocomposites was analysed for methylene blue dye. PANI/TiO_2 nanocomposite photocatalystparticles come closer in the dye solution and agglomerate, thereby reducing thesurface-active sites of photocatalyst in contact with dye solution available forphotocatalytic reaction, Photocatalytic properties of PANI/TiO_2were examined by degrading Reactive Black(MB) dye under visible light irradiation. PANI/TiO_2(10%) showed the greatest degradation (92.46%). Due to synergistic effect between PANI and TiO_2it is capable of absorbing visible light moreefficiently and decreasing the process of electron hole recombination. The nanocomposites also have significant antimicrobial activity against Streptococcus aureus, Klebsiella pneumoniae, Pseudomonas aeruginosa and Fungi Candida albicans, Aspergillus niger, Aspergillus Flavus.
Keywords: *PANI/TiO_2, Nanocomposites, Photo degradation, antimicrobial activity*

1. INTRODUCTION

The extensive production and utilization of synthetic dyes including textile industries lead to the generation of large volumes of dye-containing effluents [1, 2]. A significant concern is that a portion of these dyes remains unreacted during the dyeing process and is often discharged directly into the environment, posing serious threats not only to aquatic ecosystems but also to the broader ecological balance [3]. Furthermore, untreated dye wastes frequently decompose into poisonous and toxic chemicals, generating carcinogens that persist in the environment. Many of the organic dyes utilized in industries are either slow to biodegrade or non-biodegradable [4]. To mitigate toxic organic pollutants and complex compounds in effluents, various physicochemical methods have been employed, including photochemical oxidation, electrochemical destruction, coagulation, and adsorption on activated carbon [5]. However, these methods present significant drawbacks, such as high costs, the production of secondary pollutants, and the generation of unnecessary and toxic byproducts. In recent years, semiconductor photocatalysts have gained significant attention for the photodegradation of dyes due to their ability to generate reactive species under light irradiation [6]. Photocatalysis is defined as the enhancement of a photoreaction through the presence of a catalyst. In these reactions, the catalyst absorbs photons from light irradiation and generates electron-hole pairs. These photo-generated electrons and holes, located at the conduction band (CB) and valence band (VB) of the catalyst, respectively. They facilitate reduction and oxidation reactions which help in breaking down CO_2, H_2O and organic pollutants [7].

Hospitals are key environments for the emergence and spread of infections, particularly among immunocompromised patients. Healthcare-associated infections, resulting from bacteria, viruses, and fungi, pose a serious threat to patient safety and public health. Photocatalytic surface coatings are considered a promising solution for eliminating pathogens from frequently touched surfaces in hospital environments [8]. These coatings, in addition to their application in dye degradation, offer antimicrobial capabilities that can help reduce the transmission of infectious agents in healthcare settings. Thus, the

dual role of photocatalytic materials in both environmental remediation and microbial control highlights their significance in addressing current global health and ecological challenges.

Richard Feynman introduced the term "nanotechnology" during his lecture "There's Plenty of Room at the Bottom." Since then, the field has advanced significantly across various areas, including energy, environment, and biomedical applications [9]. Nanomaterials are defined as particles with grain size 1 to 100 nm. Due to this smaller particle size, they have unique optical, electrical, chemical and magnetic properties [10]. Metal oxide nanoparticles (NPs) possess unique properties and morphologies that make them suitable for a wide range of applications [11]. The photocatalytic activity of nano TiO_2 was first demonstrated by Fujishima and Honda in 1972. In the 1980s, its potential for environmental remediation emerged when Frank and Bard used TiO_2 powder to remove cyanide ions from an aqueous solution [12]. $TiO_2$is the most widely investigated photocatalyst due to its low cost, easy availability, large surface area, high corrosion resistance and biocompatibility [13]. However, the rapid recombination rate of charge carriers and the wide band gap energy are major limitations, restricting TiO_2 to absorb only the lower wavelength region of the electromagnetic spectrum. So, many researchers have focused on enhancing its absorption capability to extend into the visible light region by doping with metals, non-metals as well as by forming nanocomposite [14]. Nanocomposites exhibit a synergistic effect, as they combine and enhance the individual properties of their constituent nanoparticles. This interaction often leads to improved performance, such as increased stability, enhanced photocatalytic activity, and broader light absorption, making them more effective than single-component materials [15].The integration of TiO_2 with various metal oxides to form nanocomposites such as SnO_2, ZrO_2, ZnO, Bi_2O_3, WO_3, Cu_2O, CeO_2, and In_2O_3exhibits improved charge separation, an extended light absorption range, and increased surface reactivity. These synergistic effects make them highly suitable for environmental and energy-related applications [16].

In recent years, conducting polymers such as polyaniline, polypyrrole and polythiophene have been employed in photocatalysis to improve the visible-light photocatalytic performance due to their good charge carrier mobility, strong absorption in the visible range, and effective hole-accepting ability [17, 18]. Among them, polyaniline (PANI) has emerged as a preferred conducting polymer due to its simple synthesis process, low cost, non-toxic nature, and easily tunable surface chemistry [6]. Naik, Y. V. et al. [19] synthesized TiO_2/PANI nanocomposites and studied the influence of varying TiO_2 weight percentages on their performance for supercapacitor applications. J. Kalaiarasi et al. [20] prepared polyaniline/ TiO_2 nanocomposites via in situ chemical oxidative polymerization and demonstrated their enhanced diazepam sensing ability and strong antibacterial and antifungal activities.

In this work, we have synthesized PANI/TiO_2 nanocomposites by using chemical oxidative polymerization method with various concentrations of TiO_2 (5 %, 10 %, 15 % and 20 %). Then, the photocatalytic degradation kinetics of methylene blue was analysed using the PANI/TiO_2 nanocomposite. Furthermore, the antimicrobial activity of the PANI/TiO_2 nanocomposites was evaluated against Streptococcus aureus, Klebsiella pneumoniae, Pseudomonas aeruginosa and Fungi Candida albicans, Aspergillus niger, Aspergillus Flavus.

2 MATERIALS AND METHODS

2.1 Synthesis of Polyaniline

Polyaniline (PANI) was synthesized using the in-situ chemical oxidative polymerization method. Initially, 9 mL of aniline (1 M) was mixed with 3 mL of hydrochloric acid (1 M) and stirred for 20 minutes to form aniline hydrochloride. Subsequently, 0.1 M ammonium persulfate (APS), was added dropwise to the solution under continuous stirring at 50 °C. The polymerization process was maintained for 4 hours to ensure complete conversion. The resulting precipitate was filtered, thoroughly washed with deionized water and acetone, and then dried in an oven at a constant temperature for 24 hours to yield a homogeneous polyaniline composite.

2.2 Synthesis of PANI-TiO_2 Nanocomposites

The PANI–TiO_2 binary nanocomposite was synthesized using the chemical oxidative polymerization method, in which aniline monomer was polymerized in the presence of TiO_2, hydrochloric acid (HCl), and ammonium persulfate (APS) used as the oxidizing agent. The TiO_2-to-aniline molar ratios were varied at 5%, 10%, 15%, and 20%. Initially, 20 mL of 0.2 M APS solution was added dropwise to a 0.1 M aniline hydrochloride solution containing TiO_2 nanoparticles, while maintaining the mixture in an ice bath to control the reaction rate. The resulting mixture was then stored in a refrigerator for 24 hours to ensure

complete polymerization. The precipitate was subsequently filtered and washed multiple times with distilled water until a clear filtrate was obtained. Finally, the product was dried at 80 °C for 3 hours. Four different nanocomposite samples were thus prepared and stored for further characterization.

3. RESULTS AND DISCUSSIONS

3.1 Powder X - Ray Diffraction (PXRD) analysis

The X-ray diffraction (XRD) analysis was carried out using a Philips powder diffractometer (Model PW1710), equipped with Cu-Kα radiation (λ = 1.5406 Å) as the X-ray source.The X-ray diffraction (XRD) pattern of the synthesized pure PANI–TiO_2 nanocomposites is presented in Figure 1. The pattern exhibits eight prominent peaks located at 2θ values of 27.14°, 35.79°, 40.96°, 54.07°, 56.37°, 62.52°, and 68.77°, which correspond to the (101), (101), (104), (111), (200), (211), (204), and (215) crystal planes, respectively. These reflections are characteristic of the tetragonal phase of TiO_2 and align well with the standard data provided by the JCPDS card no: 89-4920 [21]. The average crystallite size of the TiO_2 nanoparticles was determined using the Debye–Scherrer equation.

$D = K\lambda / \beta \cos\theta$

Where,

D - average crystal size

λ - wavelength of the X-ray radiation

K - dimensionless shape factor (Cu Kα took as 0.9)

β - line width at half-maximum intensity (FWHM)

θ - Bragg's angle.

The average particle sizes of PANI/TiO_2 nanocomposites with varying TiO_2 loadings (5%, 10%, 15%, and 20%) are found to be 28.06 nm, 16.10 nm, 21.85 nm, and 23.09 nm, respectively. The corresponding values of macrostrain, average d-spacing, and dislocation density are presented in Table 1.

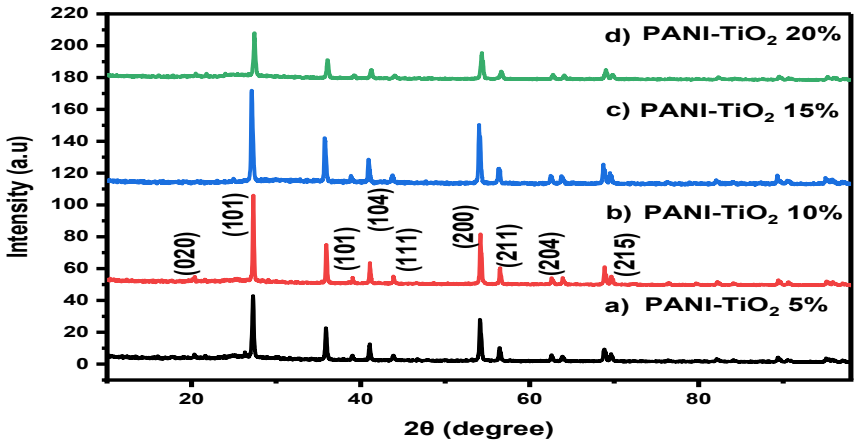

Figure 1. XRD Spectra of PANI/ TiO_2 nanocomposites

Table 2 PXRD: Crystallite size calculation

Nano composites	Parameters K	λ(Å)	Peak Position 2θ (°)	intercept c=kλ/D	Average Crystallite Size D(nm)	Slope m	Micro Strain(ε) X10^{-3}	Average d-spacing (Å) $d_{hkl}=\lambda/(2\sin\theta)$	Dislocation density(δ) X 10^{15} nm^2
TiO_2-PANI 5%	0.94	1.5406	0.0037	0.0051	28.06	0.0004	0.99	2.02	1.86
TiO_2-PANI 10%	0.94	1.5406	0.0007	0.008	16.10	0.002	0.0015	1.98	2.46
TiO_2-PANI 15%	0.94	1.5406	27.14	0.0006	21.85	0.0002	0.25	2.11	5.16

TiO_2-PANI 15%	0.94	1.5406	27.14	0.0006	23.09	0.0013	1.36	2.05	6.09

3.2 Fourier Transform Infrared (FTIR) analysis

FTIR spectra were recorded using a Shimadzu model 8400S spectrometer to analyse the functional groups and molecular interactions present in the samples. Figure 2 presents the FTIR spectra of PANI/TiO_2 nanocomposites synthesized with varying concentrations of TiO_2. The absorption bands in the 400–700 cm^{-1} region are characteristic of Ti–O–Ti stretching and bending vibrations [22]. The figure illustrates that the N–H stretching band of PANI, originally observed at 3423 cm^{-1}, gradually shifts to higher wavenumbers with increasing concentrations of TiO_2 nanoparticles [23]. The observed shifts in absorption frequencies of the composite can be attributed to strong interfacial interactions between the nanoparticles and the polar segments of PANI. This indicates that aniline monomers have been effectively polymerized on the surface of TiO_2.

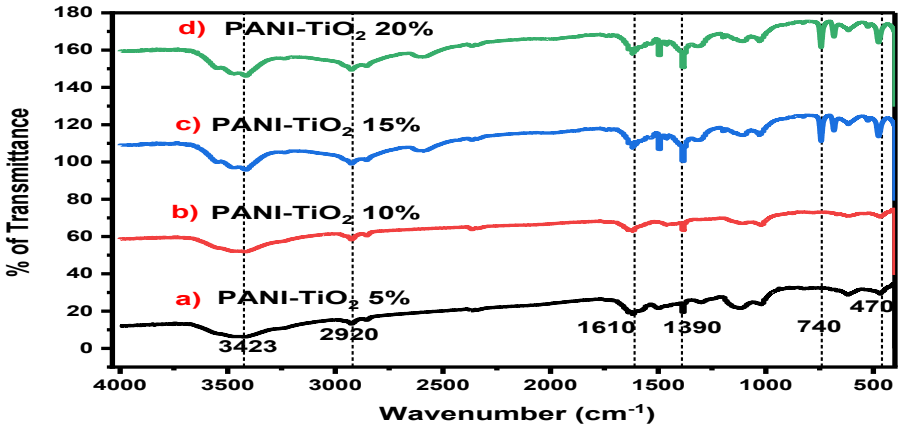

Figure 2. FTIR spectra of PANI/TiO_2 nanocomposites

3.3 UV - Vis Spectroscopy analysis

The UV-Vis diffuse reflectance spectra (DRS) of the samples were obtained using a Jasco V-600 spectrophotometer, operating within the wavelength range of 200 to 900 nm. The figure 3 shows the UV-vis absorption spectra of TiO_2 and PANI/TiO_2 nanocomposites with varying TiO_2 loading levels. All samples demonstrated strong absorption in the UV region. The optical absorption peaks for the PANI/TiO_2 nanocomposites with varying TiO_2 concentrations (5%, 10%, 15%, and 20%) were observed at 374 nm, 378 nm, and 445 nm; 381 nm, 394 nm, and 438 nm, respectively. As the TiO_2 content increased, the absorption intensity within the 200 – 400 nm range also increased, which could be attributed to the π–π* transitions of the aromatic rings present in PANI [24, 25].

The optical band gap (Eg) can be estimated using the absorption coefficient (α), which is evaluated as a function of the incident photon energy (hν). This relationship is commonly represented by the equation:

$(\alpha h\nu) = A\,(h\nu - E_g)_n$

Where,

α - absorption coefficient

h - Planck's constant

ν - frequency of the incident light

E_g - the material's band gap energy

m - exponent that indicates the nature of the electronic transition (e.g., direct or indirect).

The band gap values of the PANI/TiO_2 nanocomposites were found to be 2.90 eV, 2.93 eV, 2.84 eV, and 2.47 eV, respectively. A slight increase in the band gap is observed for the 10% of TiO_2 loaded sample, while a reduction is seen in the other two samples. A narrower band gap is generally more advantageous for promoting the generation of photoexcited charge carriers.

The Urbach energy (Eu), derived from the exponential tail of the absorption edge, provides insight into the degree of structural disorder and the presence of localized states in the material. As depicted in Figure 5, the Urbach energy of the PANI/TiO_2nanocomposites showed a decreasing trend with increasing TiO_2content. Specifically, the Eu value for the PANI-TiO_2(5%) composite was 317 meV, which decreased to 200 meV, 195 meV, and 192 meV for 10%, 15%, and 20% TiO_2loadings, respectively.

This reduction in Urbach energy suggests a systematic decrease in structural disorder and defect states within the nanocomposites. The incorporation of TiO_2nanoparticles appears to promote better polymer chain ordering and reduce the amorphous content in the PANI matrix.

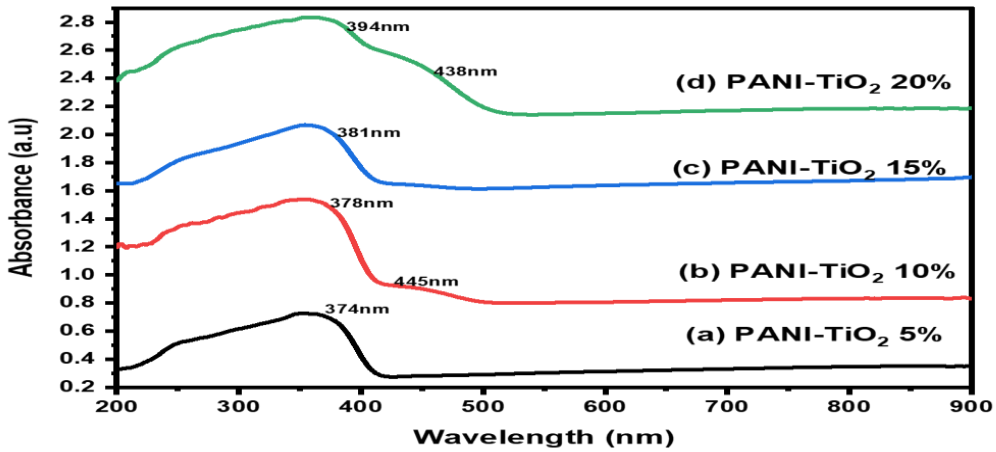

Figure 3. UV-Visible spectrum of PANI/ TiO_2 nanocomposites

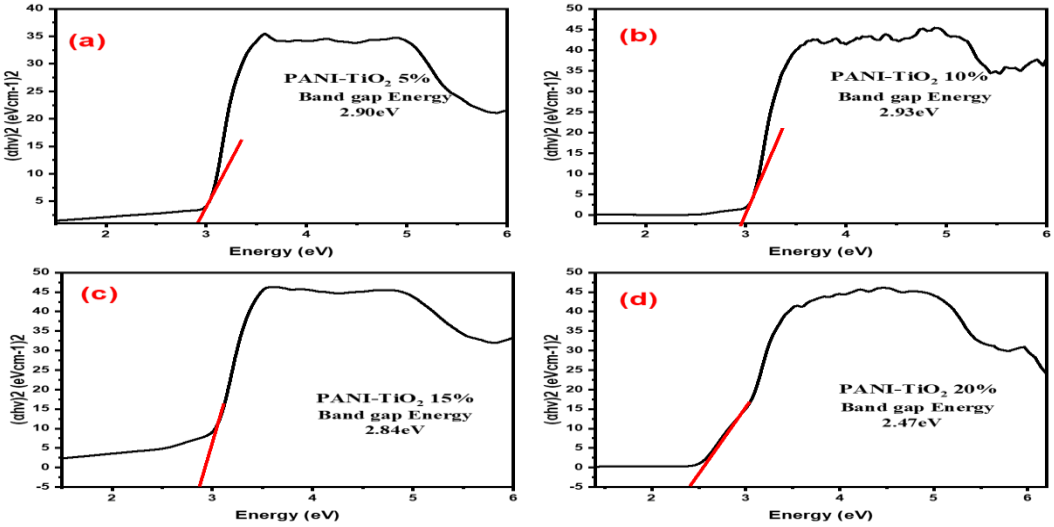

Figure 4. Bandgap energy of PANI/ TiO_2 nanocomposites

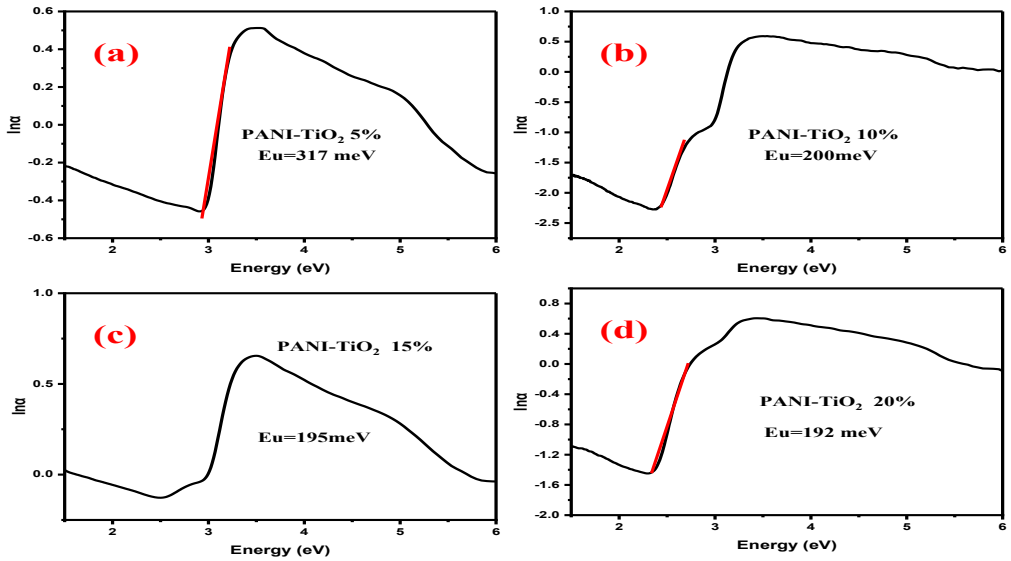

Figure 5. Urbach Energy of PANI/ TiO_2 nanocomposites

Table 2 UV-DRS using Band gap and Urbach Energy.

No	Sample	UV-Vis peaks (nm)	Band gap Energy (eV) value obtained from $(\alpha hv)^2$ to (hv) plot	Urbach Energy (meV)
1	PANI/ TiO_2(5%)	374	2.90	317
2	PANI/ TiO_2(10%)	378, 445	2.93	200
3	PANI/ TiO_2(15%)	381	2.84	195
4	PANI/ TiO_2(20%)	394, 438	2.47	192

3.4.SEM with EDAX Analysis:

The SEM images revealed that the PANI-TiO_2 nanoparticles were uniformly distributed and embedded within the polyaniline matrix, forming nearly spherical-shaped particles with slight agglomeration. These spherical particles were in the nanometre scale and exhibited a smooth and interconnected surface structure, indicating strong interfacial interaction between PANI and TiO_2. The spherical morphology supports efficient charge transport and enhances the photocatalytic surface area [26 -28].

The EDAX spectrum confirmed the presence of key elements such as titanium (Ti), oxygen (O), carbon (C), and nitrogen (N), which are characteristic of TiO_2 and polyaniline. The strong peaks for Ti and O confirm the presence of TiO_2 while C and N peaks validate the successful incorporation of PANI. The homogeneous distribution of these elements suggests good dispersion of TiO_2 within the PANI matrix, which plays a critical role in enhancing visible-light absorption and charge separation [29-32].

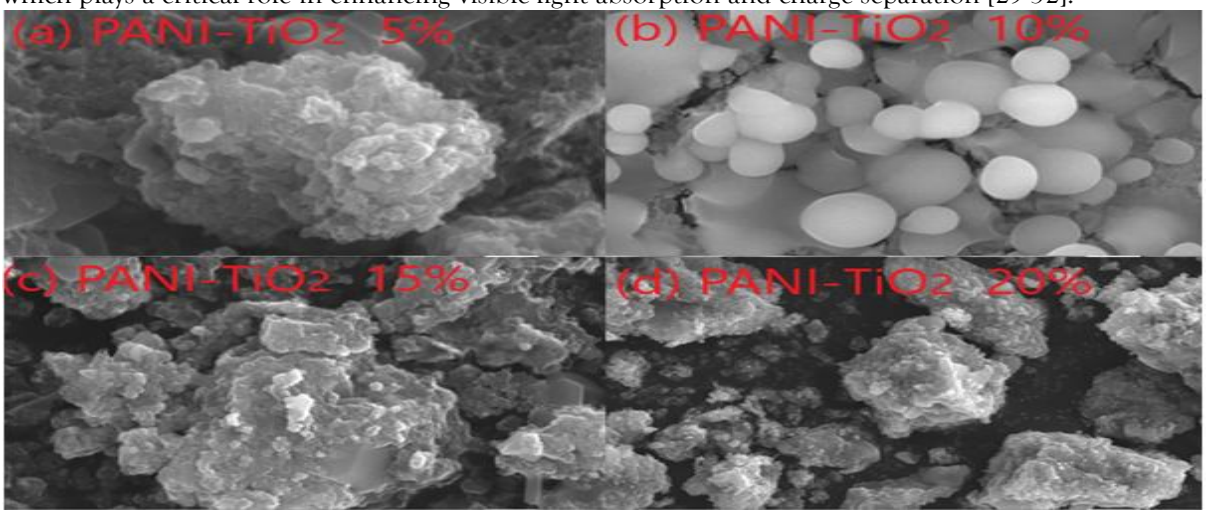

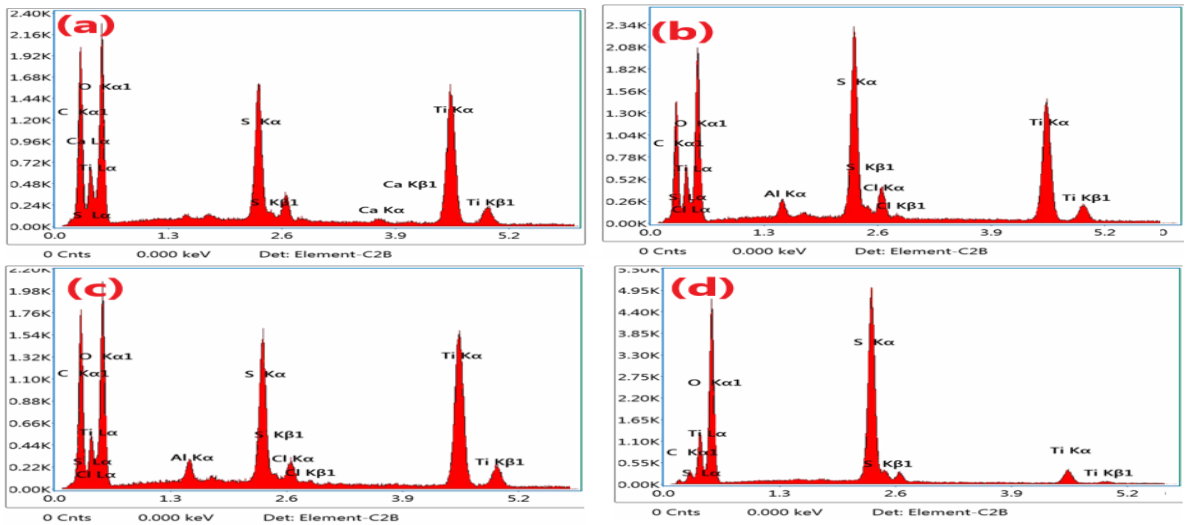

International Journal of Environmental Sciences
ISSN: 2229-7359
Vol. 11 No. 20s, 2025
https://theaspd.com/index.php

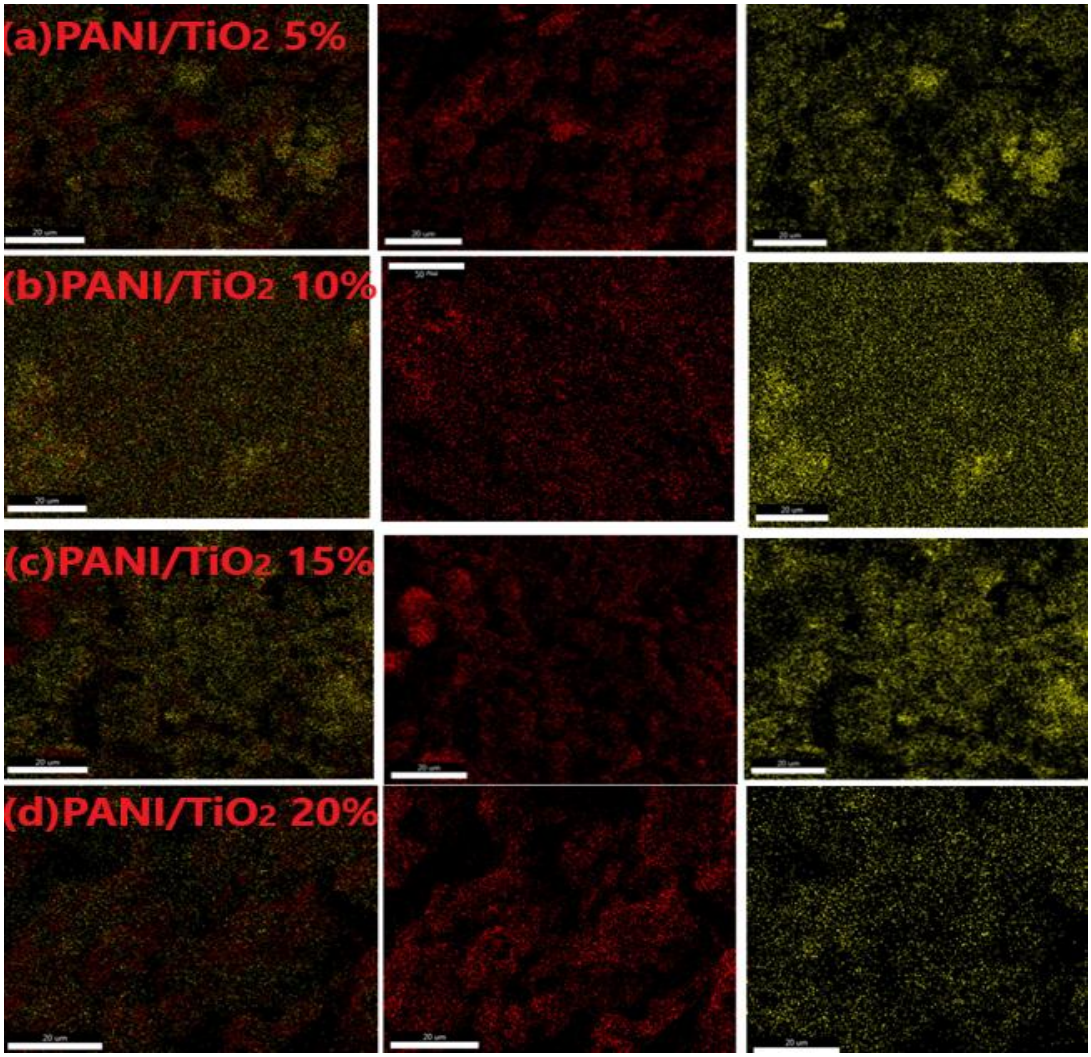

Figure 5. SEM with EDAX, Colour mapping of PANI-TiO_2nanocomposite

3.5.Average particle size analysis

The morphology and average particle size of PANI-TiO_2nanocomposites (Fig a to d)were analysed using SEM images processed through ImageJ software. All samples exhibited predominantly spherical-shaped particles, indicating uniform growth and good compatibility between PANI and TiO_2. Fig a. (5% PANI) showed an average particle size of 26 nm, while Fig b.(10% PANI) exhibited the smallest size of 19 nm. The reduced size in Fig b.suggests improved dispersion and stronger interfacial bonding, leading to enhanced photocatalytic properties. In contrast, Fig c.(15% PANI) and Fig d.(20% PANI) showed slightly increased particle sizes of 25 nm and 24 nm, respectively, which may be due to polymer-induced agglomeration. Despite this, the particles retained a near-spherical morphology across all samples [33,34].

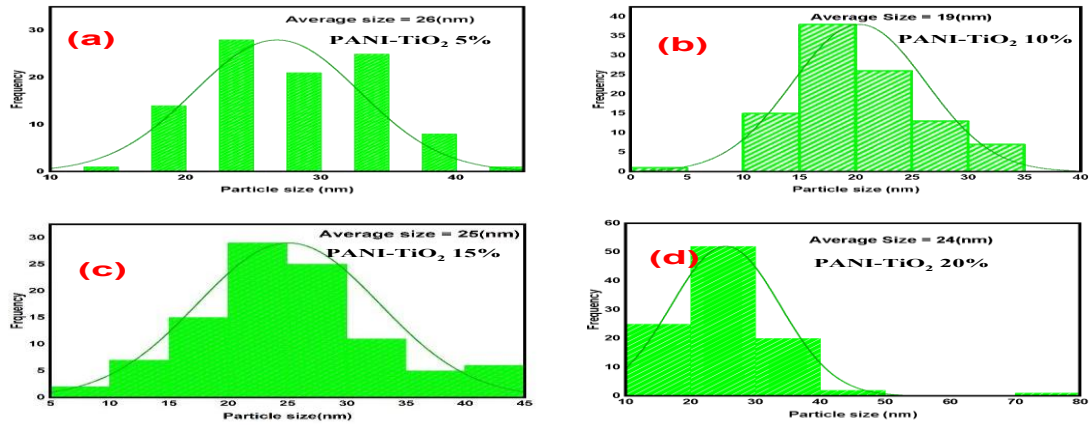

Figure 6. Average diameter analysis of PANI-TiO_2-nanocomposites

3.6. Photocatalytic activity

The photocatalytic activity of PANI-TiO_2 nanocomposites was studied with varying PANI loadings (5%, 10%, 15%, and 20%) under visible light irradiation. The results revealed that PANI incorporation significantly enhanced the photocatalytic performance of TiO_2. Among the samples, the 10% PANI-TiO_2 composite exhibited the highest photocatalytic efficiency, achieving 92.46% degradation of the target pollutant. This enhancement is mainly due to improved visible-light absorption and efficient separation of photogenerated charge carriers [35- 37].

The 5% PANI-TiO_2 nanocomposite also showed good activity, with an 83.01% degradation rate, indicating that even low levels of PANI can improve photocatalytic performance. However, when the PANI content increased to 15%, the degradation efficiency slightly decreased to 89.13%, suggesting a saturation point in the synergistic effect. At 20% PANI loading, the activity dropped further to 75.14%, possibly due to excess polymer coverage on the TiO_2 surface, which can hinder light penetration and active site exposure[38, 39].

These results confirm that 10% PANI loading provides the best balance between enhanced light absorption and efficient electron transfer. Optimizing the PANI content is crucial for maximizing the photocatalytic efficiency of TiO_2-based nanocomposites for environmental applications.

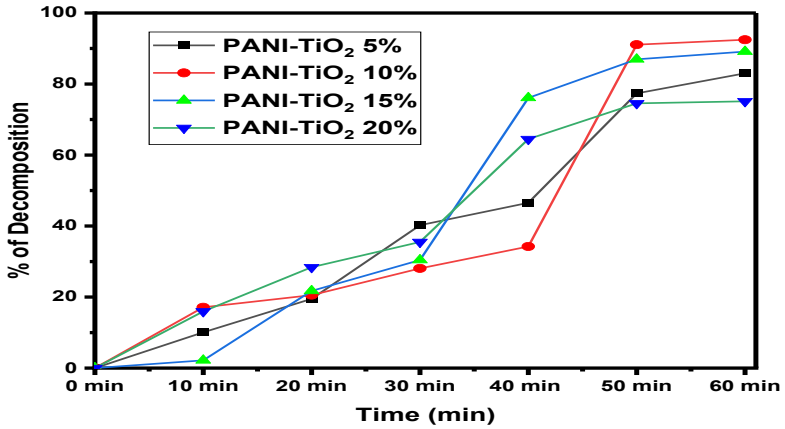

Figure 7. PANI-TiO_2 photocatalyst concentration variation a) 5% b) 10% c) 15% d) 20%

3.7.Antimicrobial activity

The antimicrobial efficacy of the PANI-TiO_2 nanocomposites was assessed using the agar well diffusion method against three bacterial strains: Staphylococcus aureus, Klebsiella pneumoniae, and Pseudomonas aeruginosa. The zone of inhibition (ZOI) was measured at concentrations of 0.1, 0.2, 0.3, and 0.4 mg/mL and compared with a standard antibiotic (positive control).

The results (Table 1) indicated concentration-dependent activity for all tested strains. Staphylococcus aureus exhibited a moderate response, with ZOI values ranging from 9 mm at 0.1 mg/mL to 11 mm at 0.4 mg/mL, compared to 15 mm for the standard. Klebsiella pneumoniae showed the highest sensitivity at 0.3 mg/mL with a ZOI of 12 mm, although it slightly decreased at 0.4 mg/mL (10 mm), indicating possible saturation effects or variability in diffusion [40-42].

Pseudomonas aeruginosa, known for its intrinsic resistance, showed the lowest inhibition at lower concentrations but reached 12 mm ZOI at 0.4 mg/mL, in contrast to 30 mm for the standard. Despite lower activity compared to standard antibiotics, the PANI-TiO_2 nanocomposites demonstrated notable antimicrobial potential, particularly at higher concentrations.

The antifungal properties of the PANI-TiO_2 nanocomposites were evaluated against Candida albicans, Aspergillus niger, and Aspergillus flavus using the agar well diffusion method. Zone of inhibition (ZOI) measurements were recorded at four concentrations (0.1, 0.2, 0.3, and 0.4 mg/mL) and compared with a standard antifungal agent (Table 5).

Candida albicans showed a consistent ZOI of 10 mm at both 0.1 and 0.2 mg/mL, which slightly decreased to 9 mm at higher concentrations (0.3 and 0.4 mg/mL). Although the activity was moderate, it remained stable across the tested doses. In comparison, Aspergillus niger exhibited the highest inhibition zone of 15 mm at 0.1 mg/mL, which gradually declined with increasing concentration-suggesting a possible concentration-related aggregation effect or interference with diffusion at higher doses [43].

Aspergillus flavus displayed a reverse trend, with the ZOI increasing from 10 mm at 0.1 mg/mL to 12 mm at 0.4 mg/mL, indicating enhanced activity with concentration. Nevertheless, the antifungal efficacy of

the PANI-TiO_2 composites was lower than that of the standard antifungal agent, which produced inhibition zones of 25–35 mm.Overall, the nanocomposites showed mild to moderate antifungal activity, with Aspergillus niger being the most sensitive at lower concentrations. These results highlight the potential of PANI-TiO_2 composites as eco-friendly antifungal materials.

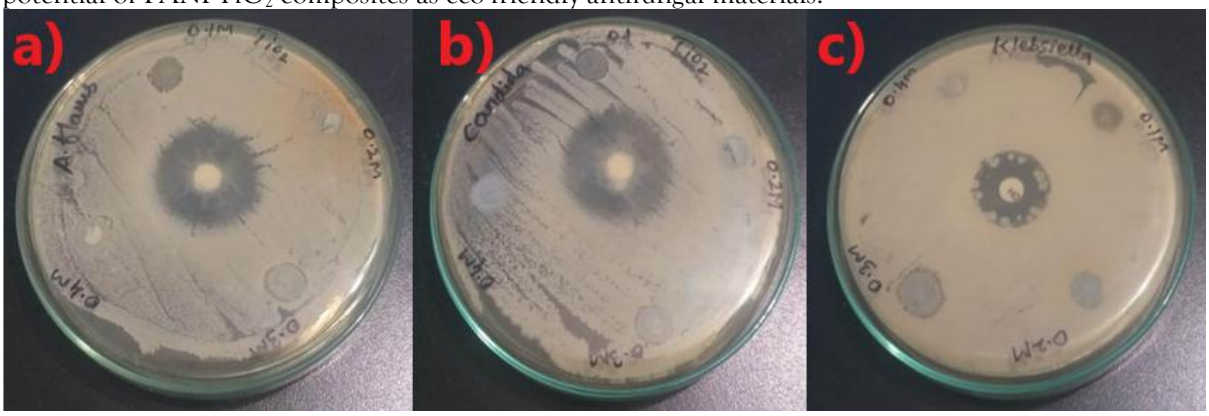

Figure 8. Antimicrobial activity PANI-TiO_2 nanocomposites

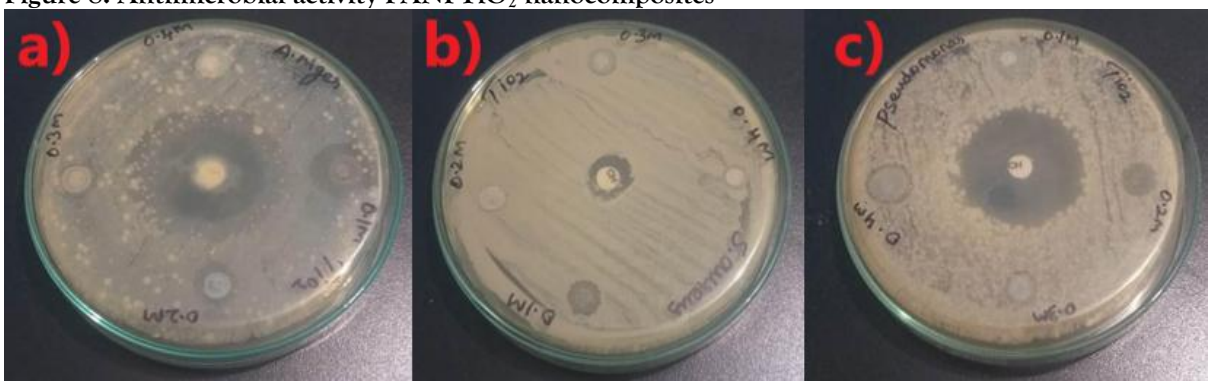

Figure 9. Antifungal activity PANI-TiO_2 nanocomposites

Table 3 Zone of inhibition (mm) at different concentrations of PANI-TiO_2

	Zone of inhibition (mm)				
Bacteria	0.1	0.2	0.3	0.4	Standard
Staphylococcus aureus	9	8	8	11	15
Klebsiella pneumoniae	9	10	12	10	20
Pseudomonas aeruginosa	9	8	8	12	30

Table 4 Zone of inhibition (mm) at different concentrations of PANI-TiO_2

	Zone of inhibition (mm)				
Fungi	0.1	0.2	0.3	0.4	Standard
Candida albicans	10	10	9	9	25
Aspergillus niger	15	14	12	13	35
Aspergillus flavus	10	10	11	12	25

4. CONCLUSION

In this study, PANI-TiO_2 nanocomposites were successfully synthesized via chemical oxidative polymerization and comprehensively characterized using UV–Vis, FTIR, XRD, and SEM techniques. The results confirmed strong interactions between PANI and TiO_2 evidenced by shifts in spectral features, reduced crystallinity, uniform dispersion, and nanoscale spherical morphology.Photocatalytic performance was evaluated through methylene blue degradation under visible light. Among the different loadings, the 10% PANI-TiO_2 composite exhibited the highest photocatalytic efficiency, achieving 92.46% degradation within 60 minutes under optimal conditions wavelength, no airflow). This superior performance is attributed to enhanced light absorption, effective charge carrier separation, and appropriate PANI content that prevents agglomeration and surface shielding.

Antimicrobial and antifungal assessments revealed that the composite showed moderate to strong activity against Staphylococcus aureus, Klebsiella pneumoniae, Pseudomonas aeruginosa, Candida albicans, Aspergillus niger, and Aspergillus flavus. The biological activity was found to increase with concentration, confirming its potential as a multifunctional agent.Overall, the PANI-TiO_2 nanocomposite demonstrates excellent potential for environmental remediationand biomedical applications, combining efficient photocatalytic degradation with notable antimicrobial efficacy. These findings suggest that such hybrid materials could serve as cost-effective, eco-friendly solutions in water treatment and infection control technologies.

REFERENCE

1. Jerin, I., Rahman, M. A., Khan, A. H., & Hossain, M. M. (2024). Photocatalytic degradation of methylene blue under visible light using carbon-doped titanium dioxide as photocatalyst. Desalination and Water Treatment, 320, 100711.
2. Sharma, S., Sharma, A., Chauhan, N. S., Tahir, M., Kumari, K., Mittal, A., & Kumar, N. (2022). TiO_2/Bi_2O_3/PANI nanocomposite materials for enhanced photocatalytic decontamination of organic pollutants. Inorganic Chemistry Communications, 146, 110093.
3. Awais, M., Khursheed, S., Tehreem, R., Uddin, S., Mok, Y. S., & Siddiqui, G. U. Ph Regulated Rapid Photocatalytic Degradation of Methylene Blue Dye Via Nitrogen-Niobium Doped Titanium Dioxide Nanostructures Under Sunlight. Available at SSRN 4089339.
4. Kumar, A., Raorane, C. J., Syed, A., Bahkali, A. H., Elgorban, A. M., Raj, V., & Kim, S. C. (2023). Synthesis of TiO_2, TiO_2/PAni, TiO_2/PAni/GO nanocomposites and photodegradation of anionic dyes Rose Bengal and thymol blue in visible light. Environmental research, 216, 114741.
5. Nekooie, R., Shamspur, T., & Mostafavi, A. (2021). Novel CuO/TiO_2/PANI nanocomposite: Preparation and photocatalytic investigation for chlorpyrifos degradation in water under visible light irradiation. Journal of Photochemistry and Photobiology A: Chemistry, 407, 113038.
6. Sambaza, S. S., Maity, A., & Pillay, K. (2020). Polyaniline-coated TiO_2 nanorods for photocatalytic degradation of bisphenol A in water. ACS omega, 5(46), 29642-29656.
7. Abdullah, H., Khan, M. M. R., Ong, H. R., & Yaakob, Z. (2017). Modified TiO_2 photocatalyst for CO_2 photocatalytic reduction: an overview. Journal of CO_2 Utilization, 22, 15-32.
8. Gizdavic-Nikolaidis, M. R., Jose, A., Stanisavljev, D. R., Marinović-Cincović, M., Marinković, D., Svirskis, D., & Swift, S. (2024). Enhanced antimicrobial activity of photocatalytic titanium oxide upon formation of composites with polyaniline via an eco-friendly and facile microwave synthesis approach. Ceramics International, 50(20), 38943-38951.
9. Kaur, H., Kumar, S., Kaushal, S., Badru, R., Singh, P. P., & Pugazhendhi, A. (2023). Highly customized porous TiO_2-PANI nanoparticles with excellent photocatalytic efficiency for dye degradation. Environmental Research, 225, 114960. https://doi.org/10.1016/j.envres.2022.114960
10. Roy, J. (2022). The synthesis and applications of TiO_2 nanoparticles derived from phytochemical sources. Journal of Industrial and Engineering Chemistry, 106, 1–19. https://doi.org/10.1016/j.jiec.2021.10.024
11. Naseem, T., & Durrani, T. (2021). The role of some important metal oxide nanoparticles for wastewater and antibacterial applications: A review. Environmental Chemistry and Ecotoxicology, 3, 59-75.
12. Kannan, K., Chanda, D., Gautam, J., Behera, A., Meshesha, M. M., Jang, S. G., & Yang, B. (2023). Hydrothermally synthesized mixed metal oxide nanocomposites for electrochemical water splitting and photocatalytic hydrogen production. International Journal of Hydrogen Energy, 48(93), 36412-36426.
13. Jerczynski, K., Lipinska, M., Raj, W., Šlouf, M., Halagan, K., Kozanecki, M., ... & Pietrasik, J. (2022). Effect of hybrid TiO_2 nanoparticles with controlled morphology on rheological properties of poly (styrene-co-acrylonitrile) nanocomposites. Materials Today Chemistry, 26, 101189.
14. Akhter, P., Nawaz, S., Shafiq, I., Nazir, A., Shafique, S., Jamil, F., ... & Hussain, M. (2023). Efficient visible light assisted photocatalysis using ZnO/TiO_2 nanocomposites. Molecular Catalysis, 535, 112896.
15. Nallusamy, S., Asaithambi, S., Pandiaraj, S., Rahaman, M., Elangovan, V., Eswaramoorthy, N., & Nandagopal, C. (2024). Cerium-modified TiO_2/g-C3N4 nanocomposites with synergistic effect on enhancing visible-light photocatalytic activity employing cationic dyes. Colloids and Surfaces A: Physicochemical and Engineering Aspects, 685, 133175.
16. Malekkiani, M., Ravari, F., Heshmati Jannat Magham, A., Dadmehr, M., Groiss, H., Hosseini, H. A., & Sharif, R. (2022). Fabrication of graphene-based TiO_2@ CeO_2 and CeO_2@ TiO_2 core–shell heterostructures for enhanced photocatalytic activity and cytotoxicity. ACS omega, 7(34), 30601-30621.
17. Shetty, K., & Raj, K. (2021). Synthesized conducting polyaniline-TiO_2 based nanocomposite for corrosion control on steel 316. Materials Today: Proceedings, 38, 2493-2498.
18. Nosrati, R., Olad, A., & Najjari, H. (2017). Study of the effect of TiO_2/polyaniline nanocomposite on the self-cleaning property of polyacrylic latex coating. Surface and Coatings Technology, 316, 199-209
19. Naik, Y. V., Karidurаganavar, M., Srinivasa, H. T., Siddagangaiah, P. B., & Naik, R. (2024). Influence of TiO_2 nanoparticles during in-situ polymerization of TiO_2/PANI nanocomposites and its supercapacitor properties. Journal of Energy Storage, 97, 112874.
20. Kalaiarasi, J., Balakrishnan, D., Al-Keridis, L. A., Al-mekhlafi, F. A., Farrag, M. A., Kanisha, C. C., ... & Pragathiswaran, C. (2022). Sensing and antimicrobial activity of polyaniline doped with TiO_2 nanocomposite synthesis and characterization. Journal of King Saud University-Science, 34(3), 101824.
21. Sundrarajan, M., Bama, K., Bhavani, M., Jegatheeswaran, S., Ambika, S., Sangili, A., ... & Sumathi, R. (2017). Obtaining titanium dioxide nanoparticles with spherical shape and antimicrobial properties using M. citrifolia leaves extract by hydrothermal method. Journal of Photochemistry and Photobiology B: Biology, 171, 117-124.

22. Rahman, K. H., & Kar, A. K. (2020). Titanium-di-oxide (TiO_2) concentration-dependent optical and morphological properties of PAni-TiO_2 nanocomposite. Materials Science in Semiconductor Processing, 105, 104745.
23. Ramesan, M. T., & Sampreeth, T. (2017). Synthesis, characterization, material properties and sensor application study of polyaniline/niobium doped titanium dioxide nanocomposites. Journal of Materials Science: Materials in Electronics, 28, 16181-16191.
24. Zhao, H., Li, Z., Lu, X., Chen, W., Cui, Y., Tang, B., ... & Wang, X. (2021). Fabrication of PANI@ TiO_2 nanocomposite and its sunlight-driven photocatalytic effect on cotton fabrics. The Journal of The Textile Institute, 112(11), 1850-1858.
25. Sasikumar, M., & Subiramaniyam, N. P. (2018). Microstructure, electrical and humidity sensing properties of TiO_2/polyaniline nanocomposite films prepared by sol–gel spin coating technique. Journal of Materials Science: Materials in Electronics, 29(9), 7099-7106.
26. Esfandian, H., Mirzaei, S., Chari, A. S., Ghadi, R. A., & Moqadam, I. H. (2024). Photocatalytic degradation of chlorpyrifos pesticide in aqueous solution using Cu-doped TiO_2/GO photocatalysis vicinity of UV and visible light. Materials Science and Engineering: B, 305, 117385.
27. Turkten, N., Karatas, Y., Uyguner-Demirel, C. S., & Bekbolet, M. (2023). Preparation of PANI modified TiO_2 and characterization under pre-and post-photocatalytic conditions. Environmental Science and Pollution Research, 30(51), 111182-111207.
28. Venkatesan, A., Al-Onazi, W. A., Elshikh, M. S., Pham, T. H., Suganya, S., Boobas, S., & Priyadharsan, A. (2022). Study of synergistic effect of cobalt and carbon codoped with TiO_2 photocatalyst for visible light induced degradation of phenol. Chemosphere, 305, 135333.
29. Abid, N. K., & Hasan, S. M. (2022). Structural properties of prepared PANI/TiO_2 nanocomposite by chemical polymerization. Iraqi Journal of Physics, 20(3), 29-39.
30. Saeb, E., & Asadpour-Zeynali, K. (2021). Facile synthesis of TiO_2@ PANI@ Au nanocomposite as an electrochemical sensor for determination of hydrazine. Microchemical Journal, 160, 105603.
31. Sibhatu, A. K., Weldegebrieal, G. K., Sagadevan, S., Tran, N. N., & Hessel, V. (2022). Photocatalytic activity of CuO nanoparticles for organic and inorganic pollutants removal in wastewater remediation. Chemosphere, 300, 134623.
32. Mahmoud, A. A., Ali, S. B., Ajiya, D. A., & Muhammad, M. (2025). Photodegradation of some Antibiotics and Industrial Dye by Visible Light of Highly Active Synthesized PAni/TiO_2 Nanocomposite Photocatalyst. Jurnal Bio-Geo Material Dan Energi, 5(1), 28-38.
33. Sadegh, F., Modarresi-Alam, A. R., Noroozifar, M., & Mansouri-Torshizi, H. (2021). Solid-state synthesis of pani-tio2 nanocomposite: Investigation of reaction conditions, nature of oxidant and electrical properties. Express Polym. Lett, 15(1), 2-15.
34. Putri, N. P., Riska, A. M., Kusumawati, D. H., & Suaebah, E. (2025). Enhanced Photocatalytic Degradation of Congo Red Dye Using Green-Synthesized TiO_2 and PANI/TiO_2 with Papaya Leaf as Bio-Reduction. Trends in Sciences, 22(2), 9119-9119.
35. Turkten, N., Karatas, Y., Uyguner-Demirel, C. S., & Bekbolet, M. (2023). Preparation of PANI modified TiO_2 and characterization under pre-and post-photocatalytic conditions. Environmental Science and Pollution Research, 30(51), 111182-111207.
36. Xie, L., Ren, Z., Zhu, P., Xu, J., Luo, D., & Lin, J. (2021). A novel CeO_2–TiO_2/PANI/$NiFe_2O_4$ magnetic photocatalyst: Preparation, characterization and photodegradation of tetracycline hydrochloride under visible light. Journal of Solid State Chemistry, 300, 122208.
37. Abouri, M., Benzaouak, A., Elouardi, M., El Hamdaoui, L., Zaaboul, F., Azzaoui, K., ... & El Hamidi, A. (2025). Enhanced photocatalytic degradation of Rhodamine B using polyaniline-coated $XTiO_3$ (X= Co, Ni) nanocomposites. Scientific Reports, 15(1), 3595.
38. Zahornyi, M. M., Tyschenko, N. I., Ragulya, A. V., Lavrynenko, O. M., Kasumov, A. M., Melnyk, A. K., ... & Ievtushenko, A. I. (2021). Optical and photocatalytic activity of polyaniline/TiO_2 composites with anatase and P25 nanoparticles.
39. Tao, Y., Li, S., Zhao, S., Li, D., Wu, Y., Liang, Z., & Cheng, H. (2021). TiO_2/PANI/Graphene–PVA hydrogel for recyclable and highly efficient photo-electrocatalysts. Industrial & Engineering Chemistry Research, 60(28), 10033-10043.
40. Sanito, R. C., Yeh, T. H., You, S. J., & Wang, Y. F. (2021). Novel TiO_2/PANI composites as a disinfectant for the elimination of Escherichia coli and Staphylococcus aureus in aquaculture water. Environmental technology & innovation, 22, 101502.
41. Gapusan, R. B., & Balela, M. D. L. (2022). Visible light-induced photocatalytic and antibacterial activity of TiO_2/polyaniline-kapok fiber nanocomposite. Polymer Bulletin, 79(6), 3891-3910.
42. Niaz, N. A., Shakoora, A., Hussaina, F., Iqbal, M., Khalidc, N. R., Saleema, M. K., ... & Ahmada, J. (2022). Structural and electronic properties of PANI-ZnO-TiO_2 nanocomposite. J Ovonic Res, 18(5), 713-722.
43. Patil, M., Mathad, S. N., Patil, A. Y., Al-Kheraif, A. A., Naik, S., & Vellapally, S. (2025). Enhanced and proficient chitosan membranes embedded with polyaniline-TiO_2 core-shell nanocomposites for fuel-cell hydrogen storage. Turkish Journal of Chemistry, 49(3), 293-309.